ORIGINAL PAPER

Synthesis and characterization of europium-containing luminescent bioactive glasses and evaluation of in vitro bioactivity and cytotoxicity

**Guohou Miao · Xiaofeng Chen · Cong Mao ·
Xian Li · Yuli Li · Cai Lin**

Abstract Luminescent europium-containing bioactive glasses (EuBG) based on the 58 %SiO_2–33 %CaO–9 %P_2O_5 (in mass, %) system were synthesized using sol–gel technique by adding Eu_2O_3 in silica network. The structural, textural and optical properties, as well as in vitro bioactivity and biocompatibility of the material were characterized using various methods. The results show that all the Eu-containing bioactive glass materials exhibit an amorphous structure, large specific surface area, relatively uniform pore size distribution and high in vitro bioactivity, similar to the conventional sol–gel bioactive glass. More importantly, the addition of Eu_2O_3 endow the material with a luminescent property even after immersion in aqueous solution and the luminescent intensity increases with the increase of Eu_2O_3 content. The cytotoxicity assay indicates that pure EuBG extract significantly inhibit the growth of rat marrow mesenchymal stem cells (rMSCs), while 25 % concentration of the extract diluted by culture medium could significantly improve the proliferation of rMSCs in comparison with pure medium. According to the above results, the material presents excellent apatite-forming activity, luminescent property and biocompatibility, demonstrating their potential applications in the fields of bone regeneration and drug delivery system.

Keywords Sol–gel · Bioactive glass · Bioactivity · Luminescent property · Cytotoxicity

G. Miao · X. Chen (✉) · C. Mao · X. Li · Y. Li · C. Lin
School of Materials Science and Engineering, South China
University of Technology, Guangzhou 510641, People's
Republic of China
e-mail: chenxf@scut.edu.cn

G. Miao
e-mail: miaoguohou@126.com

G. Miao · X. Chen · C. Mao · X. Li · Y. Li
National Engineering Research Center for Tissue Restoration
and Reconstruction, Guangzhou 510006, People's Republic of
China

G. Miao · X. Chen
Guangdong Province Key Laboratory of Biomedical
Engineering, South China University of Technology, Guangzhou
510006, People's Republic of China

C. Lin
Department of Burn, The First Affiliated Hospital of Wenzhou
Medical College, Wenzhou 325000, People's Republic of China

1 Introduction

Since the first discovery of Bioglass® in the 1970s by Hench [1], bioactive glass (BG) and glass–ceramics have been widely studied as bone repair and tissue engineering materials [2, 3] because of their unique ability to chemically bond with both hard and soft tissues through a bone-like apatite layer formed on their surfaces [4, 5]. More remarkably, recent studies demonstrated that the dissolution ions released from BG could promote proliferation and differentiation of osteoblasts by activating a series of genes that control cellular response [6–8]. Sol–gel technique can be used to synthesize porous materials with high purity in a moderate reaction condition, which greatly improves physicochemical properties and bioactivity of BG since the first preparation of sol–gel BG in 1990 [9–11]. The sol–gel BG exhibits a superior in vitro apatite-forming ability and higher surface areas because of their internal microporous and mesoporous structure [12–15] compared with the traditional melting-derived BG, demonstrating a promising application potential in the field of bone tissue repair and drug delivery system.

It is well known that the bioactivity, mechanical and biological properties of BG are mainly related to their textures and chemical compositions which can be easily tuned by changing preparation method and introducing other metal elements (such as Mg, Sr, Zn, Cu, Li, Zr, etc.) that may play a special role on stimulating biological response of cells [16–22]. Sol–gel technique makes it easy to incorporate these functional ions into the silica-based biomaterials and many researches about ion-doped BG have been reported as described previously. Recently, lanthanide-containing luminescent biomaterials such as hydroxyapatite [23] and silica nanoparticles [24, 25] have attracted considerable attention as biological imaging agents and drug carriers owing to their non-toxicity and high stability compared to other materials (e.g. quantum dot and carbon nanotube). Shruti et al. [26] synthesized a kind of mesoporous bioactive scaffolds with cerium-containing glass. Meanwhile, europium-containing luminescent bioactive glass (EuBG) has been studied as a drug carrier using ibuprofen (IBU) as a model drug. The results showed that the luminescence intensity emitted by EuBG can be applied to track and monitor the cumulative released amount of IBU [27], suggesting a potential application in drug delivery system. However, few researches have focused on the effects of the introduction of Eu_2O_3 on structure, in vitro bioactivity and biological properties of BG. In this study, we aimed to synthesize a series of Eu-containing BG by sol–gel method with the addition amount of Eu_2O_3 within 1 wt% to reduce the potential cytotoxicity when exposed to in vivo environment and examine their physicochemical properties, in vitro bioactivity and cytotoxicity.

2 Experimental

2.1 Synthesis of Eu-containing bioactive glasses

Tetraethyl orthosilicate (TEOS), triethyl phosphate (TEP), $Ca(NO_3)_2 \cdot 4H_2O$ were purchased from Guangzhou Chemical Reagent Factory Co. Ltd (Shantou, PR China) and $Eu(NO_3)_3 \cdot 6H_2O$ was obtained from Shanghai Diyang Chemical Ltd. All chemical reagents were analytical grade without further purification. The luminescent sample with a mass composition of 58 %SiO_2–(33-x) %CaO–9 %P_2O_5– x %Eu_2O_3 (x = 0, 0.3, 0.5, 0.7, 1, denoted as EuBG-0, EuBG-0.3, EuBG-0.5, EuBG-0.7, EuBG-1) was prepared by common sol–gel method according to the literature with some modification [28]. In a typical synthesis of EuBG-1, TEOS (6.6 g), TEP (0.65 g), CN (4.04 g) and EN (0.076 g) were added in order every 30 min into the mixture solution of deionized water (4.2 ml) and hydrochloric acid (0.7 ml, 2 M) under continuous stirring. The resulting solution was

kept at room temperature for 3 day for aging and gelation. The obtained gel was dried at 60 and 120 °C for 3 day, respectively. After that, the dried gel was calcined at 700 °C for 3 h (5 °C/min) in air. Finally, the EuBG-1 particles (below 74 μm) were collected by grinding and sieving using a sieve shaker for further characterization. In addition, the other Eu-containing samples were also synthesized using the same method by adding different amounts of $Eu(NO_3)_3 \cdot 6H_2O$.

2.2 Characterization

The thermal behavior of the dried gel was characterized by thermogravimetry (TG) and differential thermal (DTA) analyses. The TG and DTA curves were obtained on a simultaneous thermal analyzer (Netzsch STA449C/3/MFC/G) under a nitrogen atmosphere at a heating rate of 10 K/min from room temperature up to 1,200 °C. X-ray diffraction (XRD) analysis were obtained on a Philips X' Pert PRO diffractometer equipped with Cu Kα (λ = 0.154 nm) radiation. N_2 adsorption/desorption isotherm was recorded on a pore size and surface area analyzer (NOVA 4200e, Quantachrome) at 77 K. Samples were outgassed for 4 h at 250 °C before the N_2 adsorption/desorption analysis. The surface area was calculated by the Barrett–Emmett–Teller (BET) method and the pore size distribution was determined from the desorption branch of the isotherms by Barrett–Joyner–Halenda (BJH) method. The excitation and emission spectra were collected on a fluorescence spectrophotometer (Hitachi F-7000) equipped with a 150 W xenon lamp as excitation source. Powder Fourier transform infrared spectroscopy (FTIR) analyses were performed on a Fourier transform infrared spectrometer (Nicolet Nexus, USA) using KBr pellet method in the scanning range of 4,000–400 cm^{-1}. Scanning electron microscopy (SEM) analyses were carried out on a Nova NanoSEM 430 (Netherlands) microscope.

2.3 Assessment of in vitro bioactivity

The assessment of in vitro bioactivity was carried out in simulated body fluid (SBF) solution as described by Kokubo et al. [29]. The ionic concentrations and buffering capacity of the SBF solution were similar to those of human blood plasma. The initial pH value of SBF solution was set at 7.40. 200 mg of samples were soaking in 200 ml SBF solution in polyethylene containers which were placed in a shaking incubator with a constant shaking speed of 120 rpm at 37 °C. After soaking for different times, the samples were collected by filtration and rinsed by acetone and deionized water three times, respectively, and then dried at 60 °C in air. The apatite formed on the surface was detected by FTIR, XRD, SEM. The ionic concentrations of

the supernatant were analyzed by inductively coupled plasma atomic emission spectrometry (ICP-AES, Perkin-Elmer Optima 5300DV, USA). Additionally, changes in pH value were also monitored by a pH meter (Basic pH meter PB-10, Sartorius).

2.4 In vitro cell viability assay

The cytotoxicity of EuBG was performed by the 3-(4,5-dimethylthiazol-2-yl)-2,5-diphenyitetr-azolium bromide (MTT) assay using EuBG-1 extract. The seventh passage of rMSCs was used for the test. The extract was prepared as follows: EuBG-1 was immersed into Dulbecco's modified Eagle's medium (DMEM) at a ratio of 10 mg/ml for 24 h at 37 °C. After centrifugation, the supernatant was filtrated by a sterilized microporous membrane filter (0.22 μm) and then diluted into different concentrations (100, 50, 25 %) by DMEM. After that, each extract was supplemented with 10 % fetal bovine serum (FBS). Cells were seeded in 96-well culture plate (4×10^3 cells/well) and incubated for 2 h at 37 °C in a humidified atmosphere of 95 % air and 5 % CO_2 to allow cells to adhere on the culture plate. Then, 200 μl of each diluted extract was added to each well and pure DMEM was used as control. After incubation for 1 and 3 days, 20 μl of MTT (5 mg/ml) was added to each well, followed by incubation at 37 °C for 4 h. Then the media was removed and 150 μl of dimethyl sulfoxide (DMSO) was added. The absorbance was measured at 490 nm using a microplate reader (Thermo 3001, Thermo Co., USA). Three specimens for each culture time point were tested and each test was performed in triplicate. The data were expressed as mean ± standard deviation and were analyzed using student's t test ($*p < 0.05$ was considered statistically significant).

3 Results and discussion

3.1 Thermal, textural and luminescent properties

The TG/DTA curves of EuBG-0 and EuBG-1 dried gels are shown in Fig. 1. It can be seen that these two samples exhibit similar thermodynamic process. About 5 % of total mass is lost before 170 °C, which can be attributed to the removal of physically absorbed water and ethanol. After that both the samples undergo two dramatic mass loss processes. The first mass loss (15 wt%) between 170 and 350 °C corresponding to an endothermic peak (at 260 °C) in the DTA curve is caused by the decomposition of residual organics. The second mass loss (about 22 wt%) starts at 350 until 700 °C with an obvious endothermic peak at 550 °C, which is ascribed to the elimination of nitrates. Finally, the mass remains almost constant up to
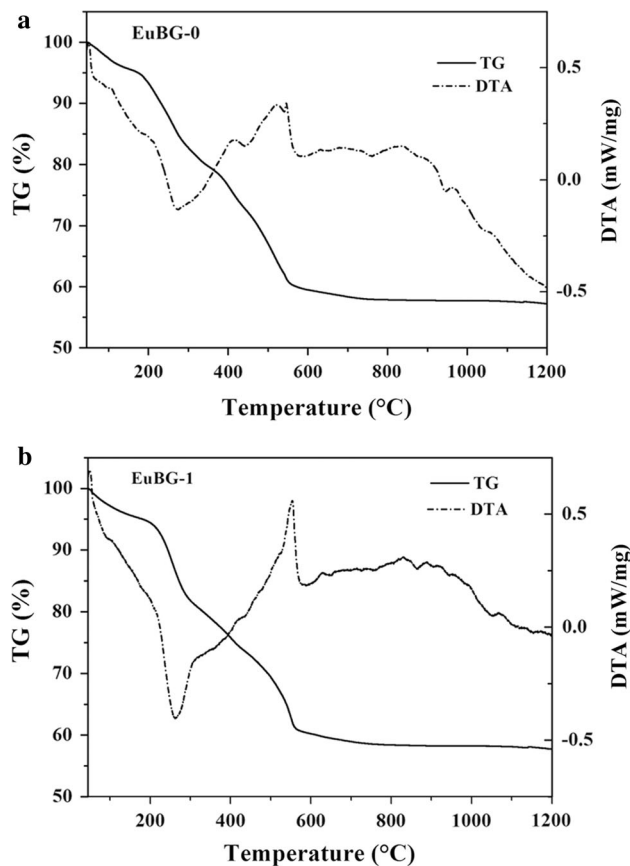

Fig. 1 TG and DTA curves of EuBG-0 (**a**) and EuBG-1 (**b**) dried gels
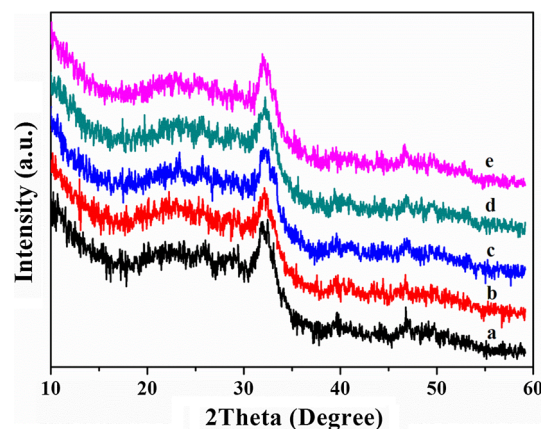

Fig. 2 XRD patterns of EuBG after calcined at 700 °C for 3 h. *a* EuBG-0, *b* EuBG-0.3, *c* EuBG-0.5, *d* EuBG-0.7, *e* EuBG-1

1,200 °C, two small exothermic peaks around 947 and 1,043 °C may be attributed to the crystallization of $CaSiO_3$ (β-wollastonite) and cristobalite [30, 31]. According to the results of TG/DTA curves, the stabilization temperature is set at 700 °C in order to completely eliminate the organic residuals and nitrates and maintain an amorphous structure. Figure 2 shows XRD patterns of EuBG after heated at 700 °C for 3 h. A broad peak at 20–30° (2θ) associated
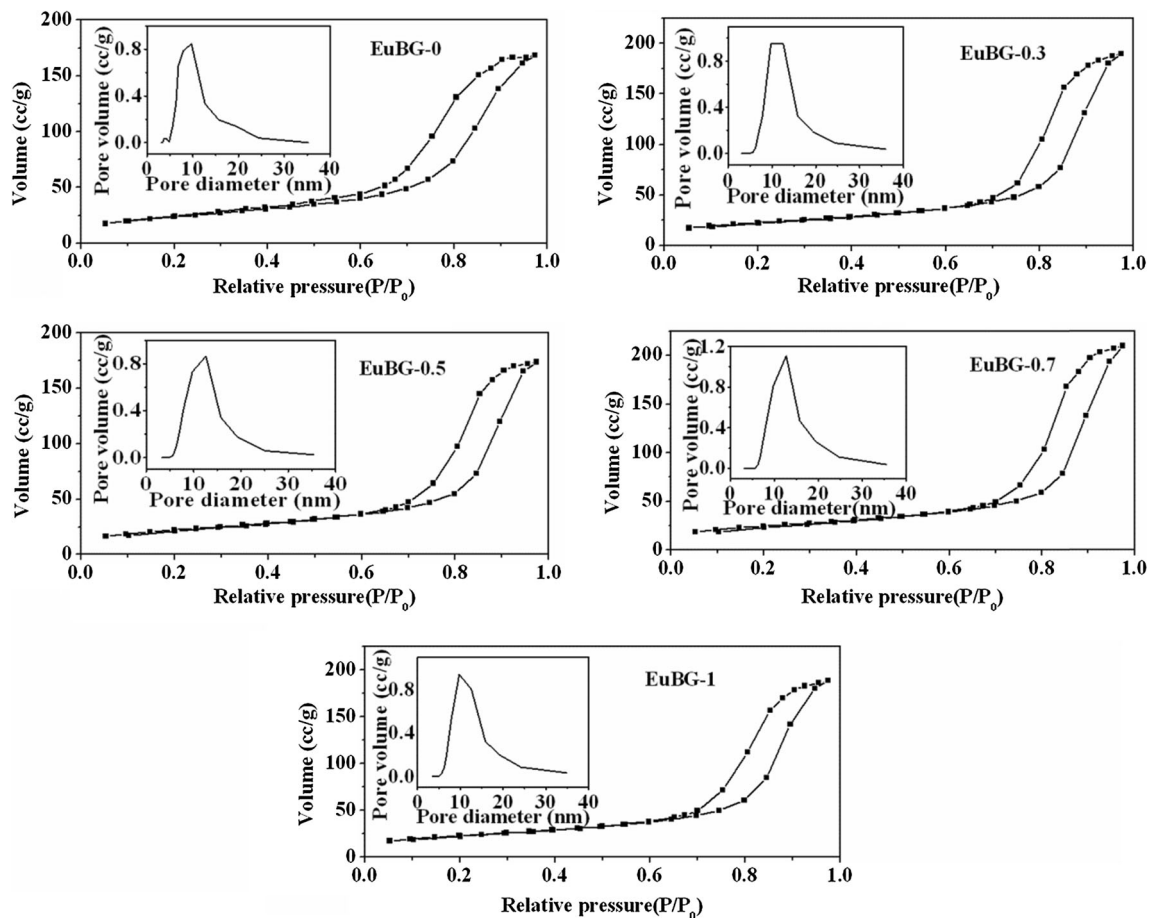
Fig. 3 N$_2$ absorption–desorption isotherms and pore size distribution curves (*inset*)

with amorphous silicate and a weak crystallization peak at $2\theta = 32°$ corresponding to the (211) reflection of apatite phase were detected in the XRD patterns of all samples, which demonstrates that all materials mainly shows glassy structure with partially crystallized phosphates.

The adsorption/desorption isotherm and pore size distribution curves of EuBG are shown in Fig. 3. All samples exhibit type IV isotherms with H3-type hysteresis loops associated with slit-shaped pores according to the IUPAC classification [32, 33]. All the pore size distribution curves (the inset of Fig. 3) show a single-peak distribution located in the mesoporous range. The specific surface areas, average pore diameter and total pore volume of EuBG are summarized in Table 1. It can be found that the surface areas of Eu-containing glasses except EuBG-0.7 are slightly lower than EuBG-0. Meanwhile, Eu-containing glasses exhibit increased total pore volume and average pore size in comparison with EuBG-0. Remarkably, sample EuBG-0.7 has the largest surface area, average pore size and total pore volume. The increase of pore diameter and pore volume may be due to the changes of Si–O–Si framework caused by the addition

Table 1 The specific surface area, pore volume and average pore diameter

Materials	Specific surface area (m^{2}g^{-1})	Average pore diameter (nm)	Total pore volume (cc/g)
EuBG-0	85.01	12.26	0.26
EuBG-0.3	80.09	14.68	0.29
EuBG-0.5	78.19	13.75	0.27
EuBG-0.7	86.35	15.01	0.32
EuBG-1	81.07	14.39	0.29

of Eu^{3+} cation which possesses higher charges and much smaller ion radius compared with Ca^{2+} cation. Two Eu^{3+} cations are needed three Ca^{2+} cations to keep the charge balance, which leads to the increase of non-bridge oxygen bond and increase the pore size and pore volume. The smaller ion size of Eu^{3+} has a stronger electrostatic effect which may tighten the network and decrease the surface areas. The pore structural parameters of the material are the combing results of these two effects, which may be
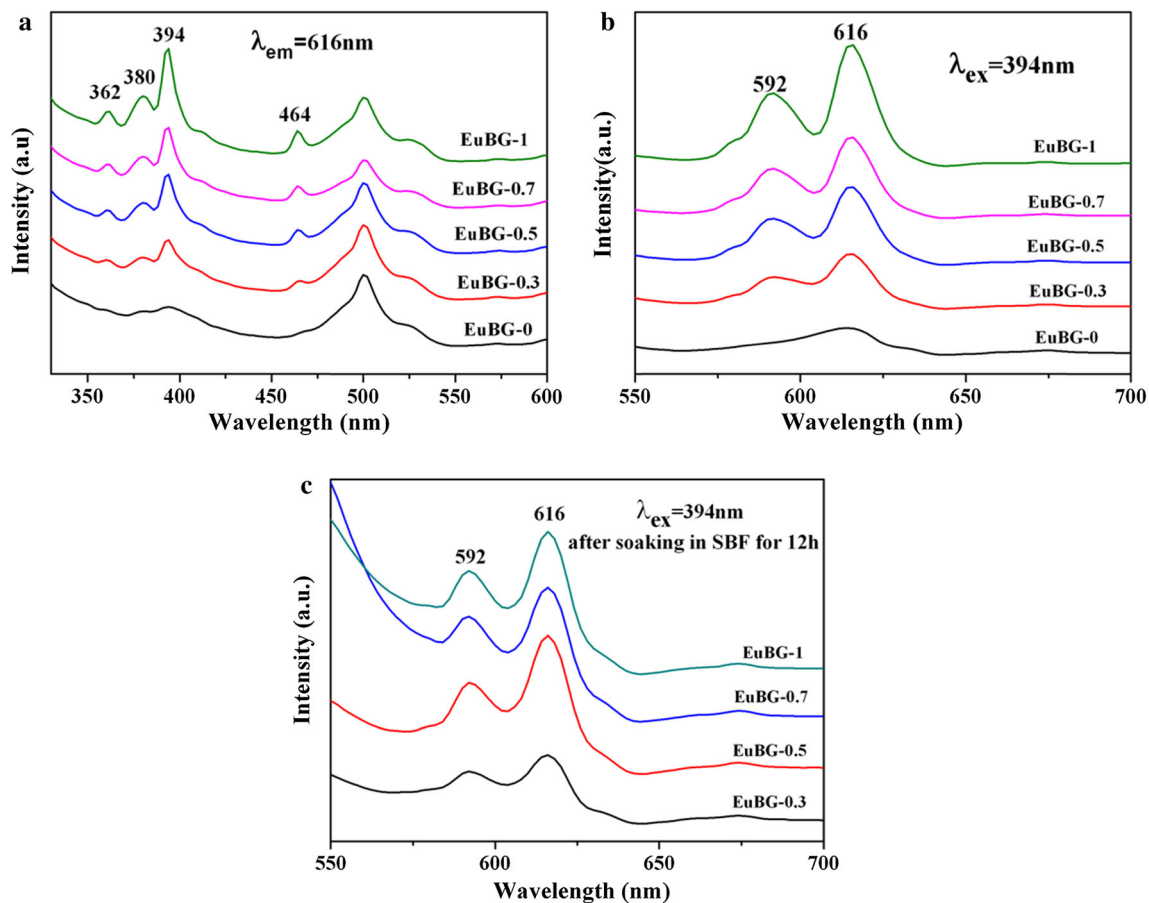
Fig. 4 Excitation (**a**) and emission (**b**, **c**) spectra of EuBG

results in the largest surface area, the pore diameter and the pore volume of EuBG-0.7. Therefore, to some extent, the pore structure parameters of samples can be tuned by changing the adding amount of Eu_2O_3.

The photoluminescence (PL) spectra of EuBG powders before and after immersion in SBF are shown in Fig. 4. The excitation spectra were monitored by $^5D_0$–$^7F_2$ transitions of Eu^{3+} ion at 616 nm (Fig. 4a). All Eu-containing glasses exhibit a maximum excitation peak at 394 nm ($^7F_0 \rightarrow {}^5L_6$) and other typical fluorescence spectra of Eu^{3+} at 360 nm ($^7F_0 \rightarrow {}^5D_4$), 382 nm ($^7F_0 \rightarrow {}^5G_4$), 464 nm ($^7F_0 \rightarrow {}^5D_2$) [23, 34]. However, no excitation peaks are observed in normal sol–gel BG. The emission spectra were detected under the excitation at 394 nm (Fig. 4b). The results show that all Eu-containing glasses present two emission peaks at 592 and 616 nm corresponding to $^5D_0 \rightarrow {}^7F_j$ transitions (j = 1, 2) of Eu^{3+}, but no emission peaks can be found in EuBG-0 sample. It can also be found that the emission intensity gradually increase with the increase of Eu_2O_3 content. It is worth noticing that the samples still show an obvious PL emission property even after soaking in SBF for 12 h (Fig. 4c), implying a

potential application in the fields of drug delivery based on their luminescent and porous properties.

3.2 In vitro bioactivity assays

Figure 5 summarizes the FTIR spectra of EuBG before and after soaking in SBF. Before soaking in SBF (Fig. 5a), the spectra are similar and present characteristic absorption bands of Si–O–Si bonds at 1,060, 798 and 465 cm^{-1} which are respectively assigned to Si–O–Si asymmetric stretching vibration, Si–O symmetric stretching and Si–O–Si symmetric bending vibrations. The weak double peaks at 605 and 566 cm^{-1} are P–O bending vibrations of phosphate in crystalline phases, which are corresponded to the XRD diffraction peak at $2\theta = 32$ °C. After soaking in SBF for 2 h (Fig. 5b), the intensities of absorption peaks at 605 and 566 cm^{-1} are intensified and a new P–O vibrational band near 963 cm^{-1} is detected, indicating the formation of a crystalline apatite layer. Moreover, the relatively weak characteristic peaks of carbonate groups at 1,450, 1,413 and 873 cm^{-1} are also detected after 2 h of soaking in SBF. The FTIR results of the samples after soaking in SBF for 2 h
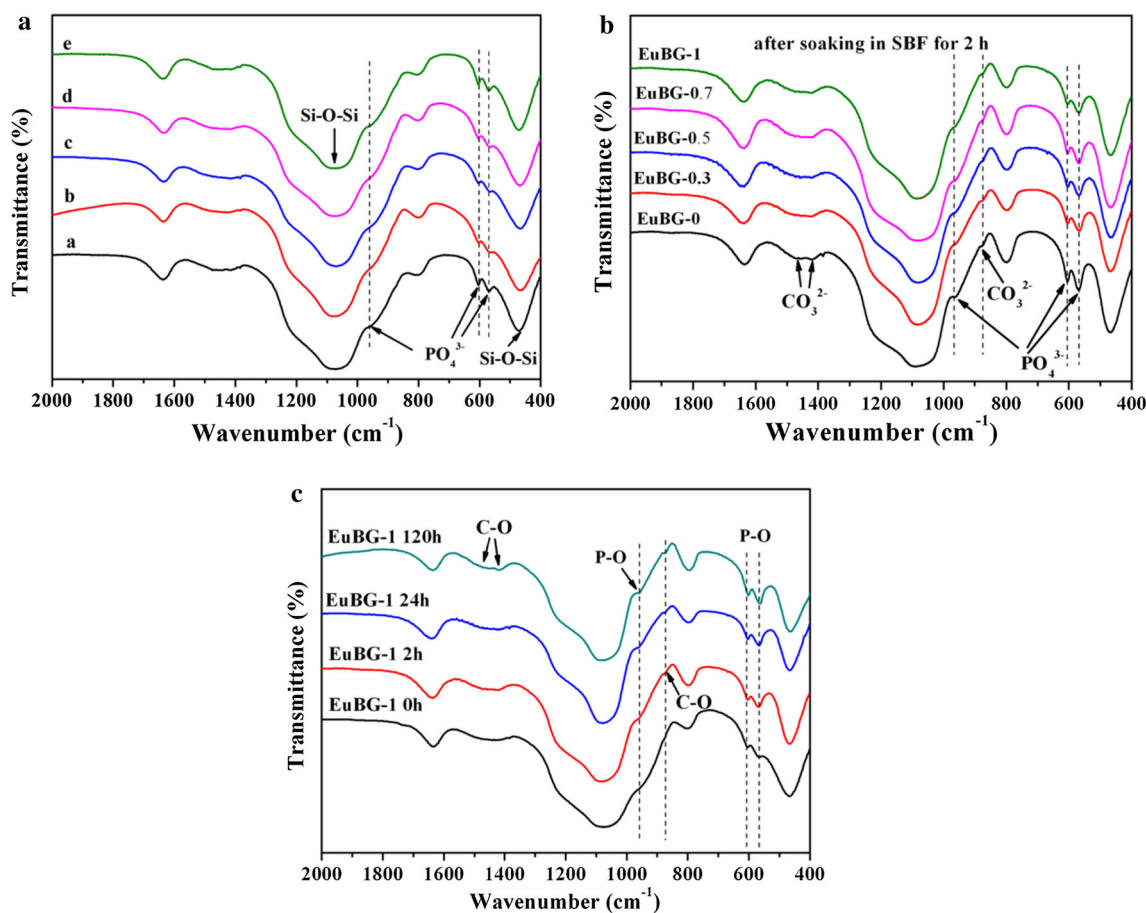
Fig. 5 FTIR spectra of EuBG before (**a**) and after (**b**, **c**) immersion in SBF solution. *a* EuBG-0, *b* EuBG-0.3, *c* EuBG-0.5, *d* EuBG-0.7, *e* EuBG-1
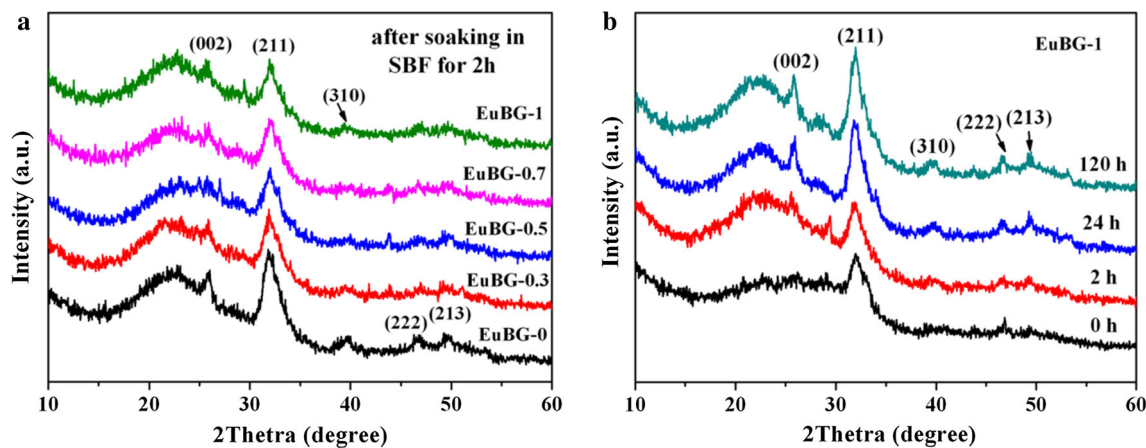

Fig. 6 XRD patterns of EuBG after soaking in SBF for 2 h (**a**) and EuBG-1 for different times (**b**)

indicate the newly formed apatite is hydroxyl-carbonate apatite (HCA). In addition, the intensities of HCA characteristic peaks gradually increase over time (Fig. 5c), indicating more and more HCA formed on the glasses surface.

Figure 6 shows the XRD patterns of EuBG after immersion in SBF for different times. Comparing with the samples before soaking in SBF (Fig. 6a), new peaks at $2\theta = 26°$, $39°$, $47°$ and $49°$ are observed after immersion in SBF for 2 h, which are assigned to (002), (310), (222) and (213) reflections of hydroxyapatite (HA) (PDF number 09-0432). Compared with Eu-containing glasses, EuBG-0 exhibits more obvious characteristic peaks of apatite,

Fig. 7 SEM micrographs of EuBG-0 (**a**) and EuBG-1 (**b**) before soaking in SBF; micrographs of EuBG-1 after soaking in SBF for (**c**) 2 h, (**d**) 24 h, (**e**) 120 h; micrographs of EuBG-0.3 (**f**), EuBG-0.5 (**g**), EuBG-0.7 (**h**) after soaking in SBF for 120 h
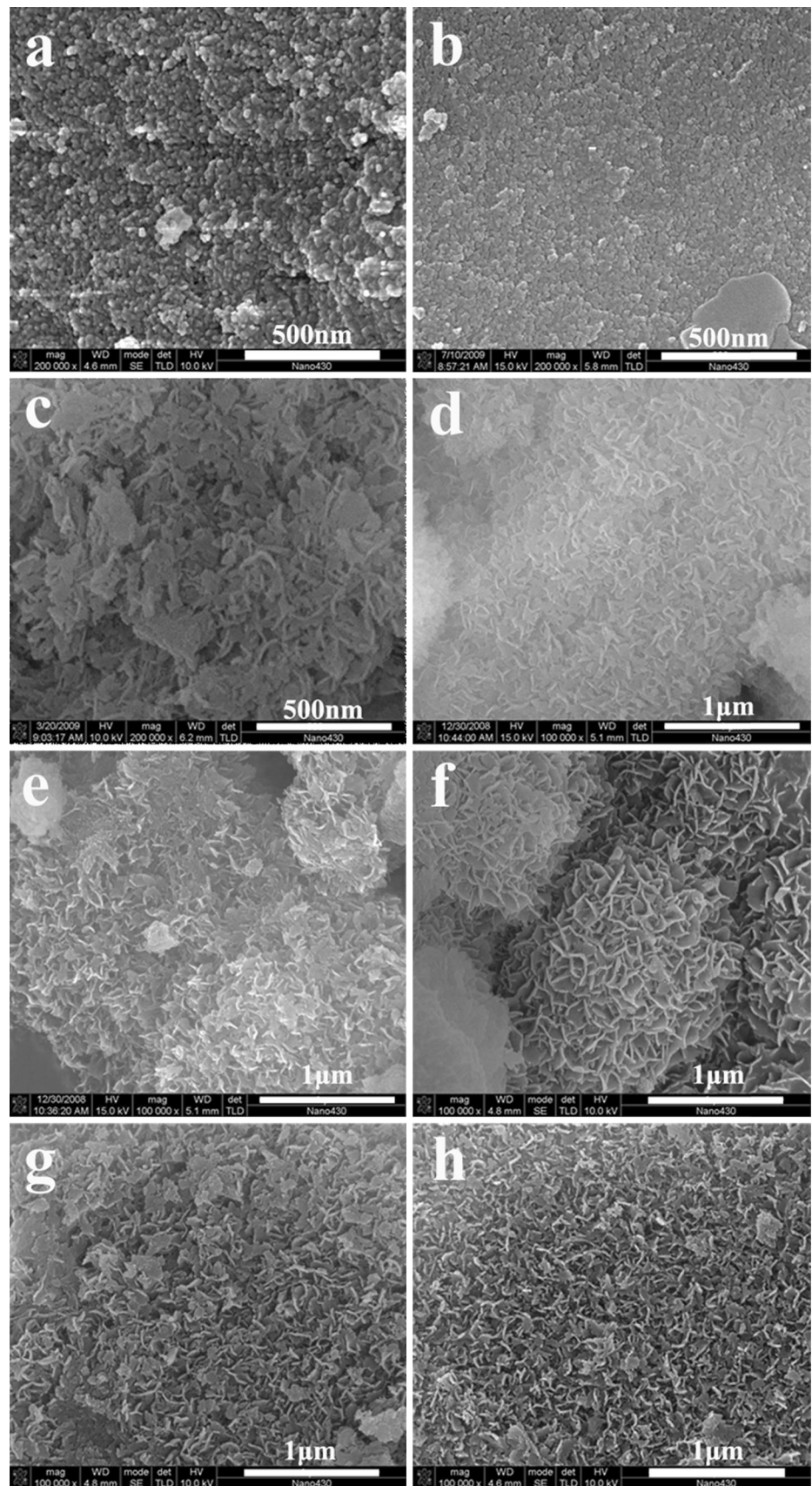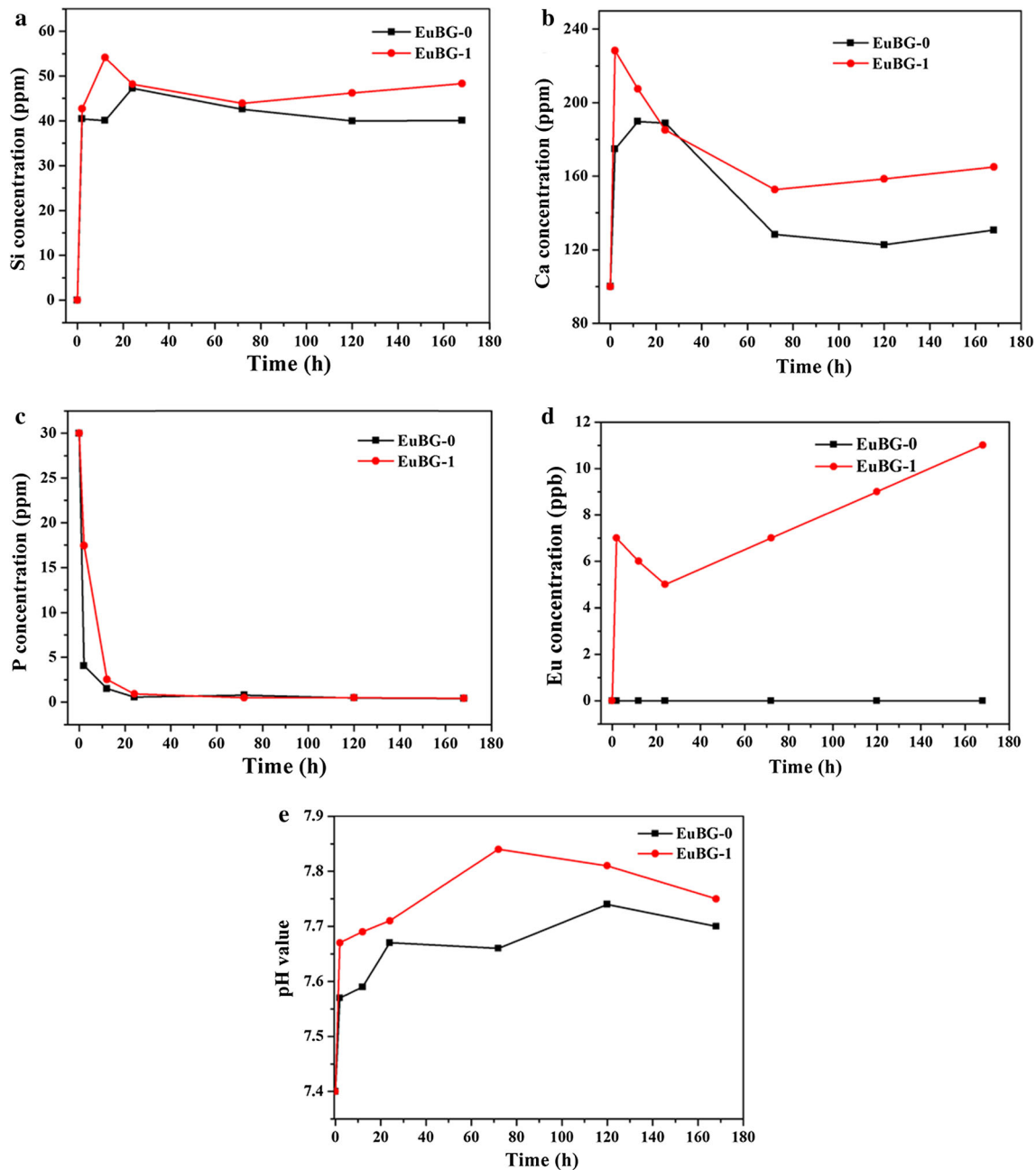
Fig. 8 Si (**a**), Ca (**b**), P (**c**), Eu (**d**) concentrations and pH values (**e**) in the SBF solution after soaking EuBG-0 and EuBG-1 powders for different times at 37 °C

demonstrating its faster apatite-forming rate. This can be explained that EuBG-0 has a higher CaO content than other Eu-containing samples because the hydroxyapatite formation rate of conventional sol–gel glasses is closely related to their chemical compositions and accelerate as the increase of soaking time, the XRD diffraction peaks become more and more intense indicating the growth of HA layer (Fig. 6b).

The surface morphologies and microstructures of EuBG before and after soaking in SBF were characterized by

SEM. As shown in Fig. 7, EuBG-0 presents a relatively smooth surface with lots of nanoscale particles before soaking in SBF (Fig. 7a) and EuBG-1 exhibit a similar surface structure (Fig. 7b). For EuBG-1, after soaking in SBF for 2 h, a rod-like apatite layer are observed on the surface (Fig. 7c), which are weak crystalline HCA according to the results of XRD and FTIR. After 24 h of immersion, the surface of EuBG-1 is completely covered by a worm-like HCA layer (Fig. 7d). As the immersion time extends to 120 h, the HCA developed into a flake-like
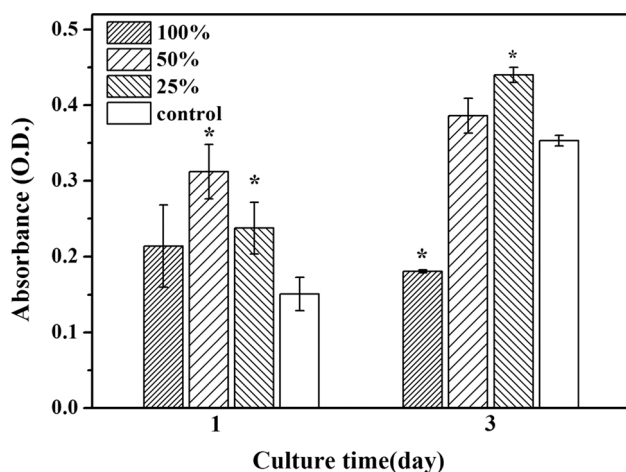
Fig. 9 Proliferation of RMSCs after cultured with serial dilutions of EuBG extracts and culture medium for 1 and 3 days

morphology (Fig. 7e). The same morphology of HCA is also observed in other Eu-containing BG (Fig. 7f–h). Based on the results of XRD, FTIR and SEM, the Eu-containing BG still possesses excellent apatite-forming ability equivalent to normal sol–gel BG, suggesting their promising application in bone regeneration.

The ionic concentrations and pH values in SBF solution as a function of soaking time for EuBG-0 and EuBG-1 are shown in Fig. 8. For Si concentration, after 2 h of rapid release, EuBG-0 and EuBG-1 reach the maximum of 47 and 54 ppm after 24 and 12 h of immersion, respectively. The release profile of Ca^{2+} ion and pH plot show a similar trend with Si release curves, and almost all the values at each time point released from EuBG-1 are a little higher than EuBG-0. During the first 12 h of immersion, P concentration displays a dramatic decrease due to the fast consumption caused by the formation of apatite, and then remains at a low level. During 7 day of soaking, there is no detection of Eu ion released from EuBG-0 while Eu concentration in SBF after immersion of EuBG-1 increases at 2 h and then keep increasing after a slight decrease during 12–24 h which may be due to the deposition of a small amount of Eu ions on the surface by electrostatic interaction with phosphate ions. Unfortunately, it is not easy to confirm the existence of Eu-containing apatite subjected to the detection limit of available technology.

3.3 Cytotoxicity test

Previous studies have demonstrated that ordered mesoporous Eu-containing BG exhibited potential biomedical application as drug carriers. Nevertheless, effects of Eu-containing BG on cell viability have not yet been studied. In this study, a preliminary experiment on cellular biocompatibility of EuBG was carried out by co-culturing

rMSCs with diluted EuBG-1 extracts. MTT tests were used to quantitatively determine the cell proliferation after cultured with the extracts. Figure 9 shows that all the extracts have a positive impact on rMSCs' growth after cultured for 1 day, especially for 50 and 25 % extracts which can significantly promote cell proliferation in comparison with the control group. After incubation for 3 days, 100 % extracts display a negative impact on the rMSCs' proliferation, which may be due to an inhibitory effect caused by the high concentration of ions, while the other extracts (50 and 25 %) show a promoting effect in cell viability. Moreover, the 25 % extract shows a significantly greater cell proliferation activity than the control group. From the above results, it is reasonable to say that ionic concentration has a great effect on rMSCs proliferation with low concentrations of ionic products presenting improved cell proliferation ability, which suggests that the dosages of EuBG should be carefully controlled in vitro cytological studies.

4 Conclusion

In this study, Eu-containing BG was successfully prepared and the physicochemical properties and cytotoxicity were investigated. Compared to Eu-free BG, the prepared EuBG exhibits amorphous structure and excellent in vitro apatite-forming ability. Additionally, the Eu-containing BG emits red luminescence of Eu^{3+} ($^5D_0 \rightarrow {}^7F_{1,2}$) under UV irradiation even after immersion in SBF, and the fluorescence intensity can be regulated by changing Eu_2O_3 content. Also, MTT assay shows that the cell viability is sensitive to ionic concentration of EuBG extracts. Therefore, the Eu_2O_3 contents should be controlled in a certain range so as to maintain the biocompatibility of EuBG.

References

1. Hench LL, Splinter RJ, Allen WC, Greenlee TK (1971) Bonding mechanisms at the interface of ceramic prosthetic materials. J Biomed Mater Res 5(6):117–141
2. Ogino M, Ohuchi F, Hench L (1980) Compositional dependence of the formation of calcium phosphate films on bioglass. J Biomed Mater Res 14(1):55–64
3. Hench L (1991) Bioceramics: from concept to clinic. J Am Ceram Soc 74(7):1487–1510

4. Greenspan D, Hench L (1976) Chemical and mechanical behavior of bioglass-coated alumina. J Biomed Mater Res 10(4):503–509

5. Wilson J, Pigott G, Schoen F, Hench L (1981) Toxicology and biocompatibility of bioglasses. J Biomed Mater Res 15(6):805–817

6. Xynos I, Edgar A, Buttery L, Hench L, Polak J (2000) Ionic products of bioactive glass dissolution increase proliferation of human osteoblasts and induce insulin-like growth factor II mRNA expression and protein synthesis. Biochem Biophys Res Commun 276(2):461–465

7. Xynos ID, Hukkanen MVJ, Batten JJ, Buttery LD, Hench LL, Polak JM (2000) Bioglass® 45S5 stimulates osteoblast turnover and enhances bone formation in vitro: implications and applications for bone tissue engineering. Calcif Tissue Int 67(4):321–329. doi:10.1007/s002230001134

8. Xynos I, Edgar A, Buttery L, Hench L, Polak J (2001) Gene-expression profiling of human osteoblasts following treatment with the ionic products of Bioglass® 45S5 dissolution. J Biomed Mater Res 55(2):151–157

9. Hench L, West J (1990) The sol–gel process. Chem Rev 90(1):33–72

10. Pereira M, Clark A, Hench L (1994) Calcium phosphate formation on sol–gel-derived bioactive glasses in vitro. J Biomed Mater Res 28(6):693–698

11. Gough J, Jones J, Hench L (2004) Nodule formation and mineralisation of human primary osteoblasts cultured on a porous bioactive glass scaffold. Biomaterials 25(11):2039–2046

12. Vallet-Regí M, Rámila A (2000) New bioactive glass and changes in porosity during the growth of a carbonate hydroxyapatite layer on glass surfaces. Chem Mater 12(4):961–965

13. Balas F, Arcos D, Pérez-Pariente J, Vallet-Regí M (2001) Textural properties of SiO_2–CaO–P_2O_5 glasses prepared by the sol–gel method. J Mater Res 16(5):1345–1348

14. Salinas A, Martin A, Vallet-Regí M (2002) Bioactivity of three CaO–P_2O_5–SiO_2 sol–gel glasses. J Biomed Mater Res 61(4):524–532

15. Arcos D, Pena J, Vallet-Regi M (2004) Textural evolution of a sol–gel glass surface in SBF. Key Eng Mater 254–256:27–30

16. Ferreira JMF, Balamurugan A, Balossier G, Kannan S, Michel J, Rebelo AHS (2007) Development and in vitro characterization of sol–gel derived CaO–P_2O_5–SiO_2–ZnO bioglass. Acta Biomater 3(2):255–262

17. El-Kheshen AA, Khaliafa FA, Saad EA, Elwan RL (2008) Effect of Al_2O_3 addition on bioactivity, thermal and mechanical properties of some bioactive glasses. Ceram Int 34(7):1667–1673

18. Ferreira JMF, Balamurugan A, Balossier G, Laurent-Maquin D, Pina S, Rebelo AHS, Faure J (2008) An in vitro biological and antibacterial study on a sol–gel derived silver-incorporated bioglass system. Dent Mater 24(10):1343–1351

19. Saboori A, Rabiee M, Mutarzadeh F, Sheikhi M, Tahriri M, Karimi M (2009) Synthesis, characterization and in vitro bioactivity of sol–gel-derived SiO_2–CaO–P_2O_5–MgO bioglass. Mater Sci Eng C 29(1):335–340

20. Zhu Y, Li X, Yang J, Wang S, Gao H, Hanagata N (2011) Composition-structure-property relationships of the CaO-MxOy–SiO_2–P_2O_5 (M = Zr, Mg, Sr) mesoporous bioactive glass (MBG) scaffolds. J Mater Chem 21(25):9208–9218

21. Ma J, Chen C, Wang D, Meng X, Shi J (2010) In vitro degradability and bioactivity of mesoporous CaO–MgO–P_2O_5–SiO_2 glass synthesized by sol–gel method. J Sol–Gel Sci Techn 54(1):69–76. doi:10.1007/s10971-010-2159-z

22. Han PP, Wu CT, Chang J, Xiao Y (2012) The cementogenic differentiation of periodontal ligament cells via the activation of Wnt/β-catenin signalling pathway by Li^+ ions released from bioactive scaffolds. Biomaterials 33(27):6370–6379. doi:10.1016/j.biomaterials.2012.05.061

23. Piaoping Y, Zewei Q, Chunxia L, Xiaojiao K, Hongzhou L, Jun L (2008) Bioactive, luminescent and mesoporous europium-doped hydroxyapatite as a drug carrier. Biomaterials 29(32):4341–4347

24. Piaoping Y, Zewei Q, Zhiyao H, Chunxia L, Xiaojiao K, Ziyong C, Jun L (2009) A magnetic, luminescent and mesoporous core-shell structured composite material as drug carrier. Biomaterials 30(27):4786–4795. doi:10.1016/j.biomaterials.2009.05.038

25. Ocaña M, Cantelar E, Cussó F (2011) A facile single-step procedure for the synthesis of luminescent Ln^{3+}:YVO4 (Ln = Eu or Er + Yb)-silica nanocomposites. Mater Chem Phys 125(1–2):224–230. doi:10.1016/j.matchemphys.2010.09.011

26. Shruti S, Salinas AJ, Lusvardi G, Malavasi G, Menabue L, Vallet-Regi M (2013) Mesoporous bioactive scaffolds prepared with cerium-, gallium- and zinc-containing glasses. Acta Biomater 9(1):4836–4844. doi:10.1016/j.actbio.2012.09.024

27. Fan Y, Yang P, Huang S, Jiang J, Lian H, Lin J (2009) Luminescent and mesoporous europium-doped bioactive glasses (MBG) as a drug carrier. J Am Chem Soc 131(10):3462–3463

28. Li R, Clark AE, Hench LL (1991) An investigation of bioactive glass powders by sol–gel processing. J Appl Biomater 2(4):231–239. doi:10.1002/jab.770020403

29. Kokubo T, Takadama H (2006) How useful is SBF in predicting in vivo bone bioactivity? Biomaterials 27(15):2907–2915

30. Roman J, Padilla S, Vallet-Regi M (2003) Sol–gel glasses as precursors of bioactive glass ceramics. Chem Mater 15(3):798–806

31. Saravanapavan P, Jones JR, Pryce RS, Hench LL (2003) Bioactivity of gel-glass powders in the CaO–SiO_2 system: a comparison with ternary (CaO–P_2O_5–SiO_2) and quaternary glasses (SiO_2–CaO–P_2O_5–Na_2O). J Biomed Mater Res Part A 66(1):110–119. doi:10.1002/jbm.a.10532

32. Sing KSW, Everett DH, Haul R, Moscou L, Pierotti RA, Rouquerol J, Siemieniewska T (1982) Reporting physisorption data for gas/solid systems with special reference to the determination of surface area and porosity. Pure Appl Chem 54(11):2201–2218

33. Lei B, Chen X, Wang Y, Zhao N, Du C, Zhang L (2009) Acetic acid derived mesoporous bioactive glasses with an enhanced in vitro bioactivity. J Non-Cryst Solids 355(52–54):2583–2587

34. Binnemans K, Van Deun R, Görller-Walrand C, Adam JL (1998) Spectroscopic properties of trivalent lanthanide ions in fluorophosphate glasses. J Non-Cryst Solids 238(1–2):11–29